NANO LETTERS

2006
Vol. 6, No. 8
1622−1626

Nanoscale Paul Trapping of a Single Electron

Dvira Segal*,† and Moshe Shapiro†,‡

Department of Chemical Physics, Weizmann Institute of Science, 76100 Rehovot, Israel, and Department of Chemistry, University of British Columbia, Vancouver V6T1Z1, Canada

Received March 12, 2006; Revised Manuscript Received June 2, 2006

ABSTRACT

We demonstrate that a Paul trap made up of four conducting nanotubes is capable of trapping a *single* electron. In addition to the size, the major differences between such a nano-trap and its macroscopic analogue are that the electron is treated as a quantum object and that its effect ("back reaction") on the trapping device cannot be ignored. We computationally demonstrate focusing and trapping of an electronic *wave packet*, while fully accounting for the image charges induced by the electron on the nanotubes. The electron image charge interaction significantly affects the electron dynamics, and thus the trap stability. An (entangled) set of trapped electrons offers a number of advantages for quantum information processing.

Trapping of individual charged particles in a small spatial region is a useful tool in many fields, such as mass spectrometry, optical spectroscopy, quantum optics, and metrology.[1] Some of the novel applications of trapped charged particles are the precise measurements of the electron magnetic moment[2] and the performance of quantum computations with a string of trapped ions.[3] Recent studies propose ion traps as transducers of nanowires' nanomechanical oscillations.[4] In the popular Penning trap, the charged particles are held in a combination of electrostatic and magnetic fields,[5] whereas in the Paul trap storage is achieved by means of high-frequency spatially shaped electrical fields.[6] Typical sizes of these devices are in the millimeter length scale, and the oscillation frequencies extend the 1−100 MHz range.

In this paper, we propose a new *nanosize* device that is demonstrated computationally to confine individual *electrons* in two or three dimensions. The proposed device, which is a nanoscale analogue of the linear Paul trap, is made up of four parallel conducting nanorods, for example, metallic carbon nanotubes (CNT), spaced symmetrically about a central axis. Application of a properly tuned ac field to the nanorods can lead to two-dimensional ("radial") confinement of the electrons at the trap center. Confinement along the third ("axial") direction can be attained by manipulating the structure of the tubes and/or the shapes of the end caps. As shown in Figure 1a, the typical dimensions of the proposed device are in the nanometric range: The distance between the tubes is $d \approx 100$ nm, each tube's radius is $a \approx 0.7$ nm, and the tubes length is $L \approx 200$ nm. These requirements are within present day technology because arrays of CNTs of precisely tailored dimensions can now be fabricated.[7] The desired conductive properties of these arrays can be achieved utilizing the new methods for nondestructive separation of semiconducting from metallic carbon nanotubes.[8,9] The device can be also fabricated from other metallic materials,

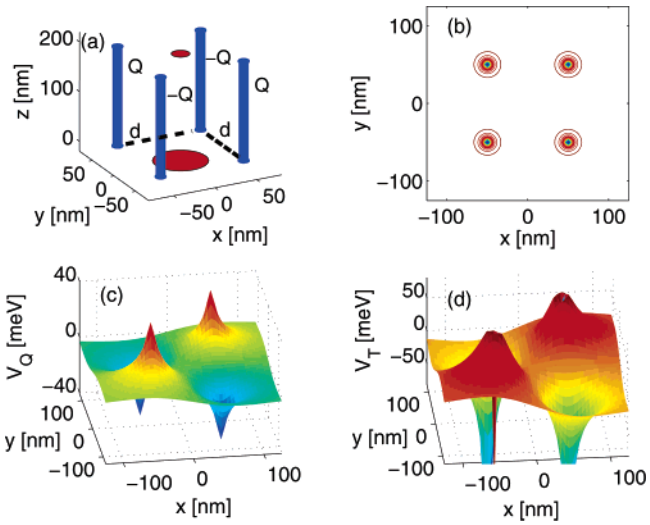

Figure 1. (a) Schematic illustration of a nano-trap composed of four parallel tubes aligned in the z direction. The large circle represents the size of the incoming electronic wave packet, and the small circle represents the size of the trapped wave packet. (b) A contour plot of $V_0(x, y)$. (c) A surface plot of $V_Q(x, y)$, for $Q/L \equiv \lambda = 0.005$ e/nm. (d) The total potential energy function for $\lambda = 0.02$ e/nm. $z = 100$ nm in panels b−d.

* Corresponding author. E-mail: ds2469@columbia.edu.
† Weizmann Institute of Science.
‡ University of British Columbia.

10.1021/nl060560h CCC: $33.50
Published on Web 06/30/2006

for example, gold[10] or palladium,[11] though such tubes' diameters are usually larger than 10 nm. The proposed device has to operate at very high frequencies, 100 GHz to 1 THz, which recent studies of the ac performance of CNT suggest are realizable.[12] Another technological issue that should be addressed is the ability to fabricate individual electrical connects in this structure. We propose doing it using synthetic methods that make feasible rational design of complex nanowire architectures.[13]

In the absence of an external potential, an electron hovering in the vicinity of the four tubes configuration is electrostatically attracted to the image charges it creates on the nanotubes. This has been shown to lead to the formation of long-lived "tubular image states".[14−17] In the context of the nano-trap, the image potential has a profound effect on the electron dynamics, resulting, as we show below, among other things, in the *reduction* of the size of the trapping stability regions.

We have calculated numerically the image potential interaction energy $V_0(x, y, z)$, including the electrostatic interaction between the rods, using the method of ref 17. A contour plot of this potential using the typical dimensions given above is displayed in Figure 1b. The depth of the potential at the center point is ~ -0.5 meV, whereas near the surface of each tube it goes down to -250 meV. It can be shown that far from the tubes ends, $z \approx 100$ nm, the axial variation of the potential is weak in comparison to the radial gradient.[17] In discussing 2D confinement, we shall ignore the axial dependence of the potential, which is permissible if the tubes are long enough.

We next consider connecting the four tubes to an external (ac or dc) source. As shown in Figure 1a, we form a quadrupole by charging tube no. 1 and its diagonal counterpart, tube no. 4, by $+Q$ and tube no. 2 and diagonal counterpart, tube no. 3, by $-Q$. We can calculate $V_T(x, y, z)$, the total interaction energy of a charged particle with the nano-quadrupole in the presence of image charges by using a simple extension of our numerical procedure.[17] It is convenient to decompose V_T into two terms, $V_T = V_0 + V_Q$, where V_0, which is independent of Q, is the image potential discussed above, and V_Q, the "charging" potential, is the additional potential resulting from the added quadrupolar charges. We have verified that V_Q scales linearly with the extra charge, that is, $V_{\alpha Q} \approx \alpha V_Q$ for distances $\rho > 5$ nm away from the tubes, and it depends very weakly on the axial coordinate. The charging potential has an approximate quadrupolar spatial shape, as shown in Figure 1c. Panel d presents the combination V_T that to a good approximation sustains the quadrupolar form. We expect that in the dc charging case, the migration of the electron to one of the tubes would lead to its eventual decay onto the surface.[16] In contrast, as in conventional linear Paul traps,[6] in the ac charging case the saddle point at the center should provide a point of stability where the electron can be confined.

We can also derive approximate analytic expressions for the image potential and the charging energy. Neglecting tube−tube polarization effects, we approximate the image potential for *infinitely* long tubes as[14]

$$V_0(x, y) \approx \sum_{j=1..4} \frac{2e^2}{\pi a} \sum_{n=1,3,5,\ldots} \mathrm{li}[(a/\rho_j)^n], \quad \mathrm{li}(x) \equiv \int_0^x \frac{\mathrm{d}t}{\ln(t)} \quad (1)$$

where ρ_j ($j = 1..4$) is the distance of the electron from the jth tube's center. This potential interpolates well between the long-range $\sum_j [\rho_j \ln(\rho_j/a)]^{-1}$ and the near-surface $\sum_j |\rho_j - a|^{-1}$ limits. The additional charging energy is given by[18]

$$V_Q(x, y) \approx eV_a \frac{\ln(\rho_1\rho_4/\rho_2\rho_3)}{\ln(\sqrt{2}a/d)} \quad (2)$$

where V_a ($-V_a$) is the potential applied to the 1,4 (2,3) pair. This formula goes over to the correct limit when the electron is placed on the surface of a tube. It can also be expressed in terms of the 1D charge density on the tubes, $\lambda = Q/L$. Assuming that close to each tube surface the electric field approaches the $E_\rho = \lambda/\rho$ limiting value, valid for an infinitely long, uniformly charged wire, we have that $V_Q(x, y) \approx e\lambda \ln(\rho_2\rho_3/\rho_1\rho_4)$. This analytic expression is in a good agreement with the potential obtained numerically.

We next allow for an ac charging at frequency Ω. The total potential is now a sum of a static term and an ac term

$$V_T(x, y, t) = V_0(x, y) + V_Q(x, y)\cos(\Omega t) \quad (3)$$

A more general potential could be devised by including an additional dc term, $cV_Q(x, y)$. Here we limit our investigation to the $c = 0$ case. The dynamics of a single electron subject to this potential is obtained by solving the time-dependent Schrödinger equation

$$i\hbar\partial_t\Psi(x, y, t) = \left[\frac{-\hbar^2}{2m_e}(\partial_x^2 + \partial_y^2) + V_T(x, y, t)\right]\Psi(x, y, t) \quad (4)$$

where m_e is the electron mass. Unlike the case of a pure quadrupole,[6] and because of the presence of the image charge potential (V_0), this equation is nonseparable in the x, y coordinates and the analytical results of ref 19 cannot be applied. Given eq 4, the propagation of an initial wave packet is done using the unitary split evolution operator[20]

$$U_{t+\hbar\Delta,t} = \mathrm{e}^{-i\Delta\cdot V_T(x,t+\hbar\Delta)/2}\mathrm{e}^{-i\Delta\cdot T}\mathrm{e}^{-i\Delta\cdot V_T(x,t)/2} \quad (5)$$

where T is the kinetic energy operator and $\hbar\Delta$ is the time increment. To eliminate artificial reflections of the wave function from the boundaries, we introduce into the Hamiltonian an optical potential that absorbs the scattered wavelets before they reach the grid boundaries.[21] Because of the scaling properties of the Schrödinger equation (eq 4), it is possible to design traps of various spatial dimensions operating at different control conditions. To see this, we define three dimensionless variables, $\xi = \Omega t$, $\tilde{x} = x/\alpha$, and $\tilde{y} = y/\alpha$, in terms of which we can write eq 4 as

$$i\hbar \frac{\partial \Psi(\tilde{x},\tilde{y},\xi)}{\partial \xi} = \left[\frac{-\hbar^2}{2\Omega m_e \alpha^2}\left(\frac{\partial^2}{\partial \tilde{x}^2} + \frac{\partial^2}{\partial \tilde{y}^2}\right)\right] \Psi(\tilde{x},\tilde{y},\xi) + \frac{[V_0(\tilde{x},\tilde{y}) + V_Q(\tilde{x},\tilde{y})\cos(\xi)]}{\Omega} \Psi(\tilde{x},\tilde{y},\xi) \quad (6)$$

It follows that the dynamics is invariant to the scaling up of the spatial and temporal coordinates

$$\alpha \rightarrow \sqrt{\kappa}\alpha, \quad \Delta \rightarrow \kappa\Delta \quad (7)$$

provided that the frequency, charge density, and image potential are scaled down as

$$\Omega \rightarrow \Omega/\kappa, \quad \lambda \rightarrow \lambda/\kappa, \quad V_0 \rightarrow V_0/\kappa \quad (8)$$

The scaling of the image potential, which roughly behaves as $1/[\rho \ln(\rho/a)]$, can be accomplished approximately by adjusting the tube's radii.

We are now in a position to demonstrate trapping and focusing of a single electron in the nano-trap. Figure 2 displays the time evolution of an initial (highly localized) Gaussian wave packet $\Psi(x, y, t = 0) = \exp[-(x^2 + y^2)/2\sigma^2]/\sqrt{\pi\sigma^2}$, of width $\sigma = 10.5$ nm, subject to different charging potentials and ac modulation frequency of $\nu \equiv 1/T \equiv \Omega/2\pi = 8.3\ 10^{11}$ Hz. The spatial parameters are the same as those in Figure 1. We see that the wave packet evolves into distinct shapes for different values of the applied potential: In the absence of the ac modulation, the electron accumulates in the vicinity of the tubes, as shown in Figure 2a−d. For the case of weak charging potentials, shown in Figure 2e−h, the electron is neither trapped nor is it strongly attracted to the tubes. Rather, the wave packet spreads slowly while filling the entire inter-tube space. Tight focusing occurs when the charging is high enough in Figure 2i−l with the wave packet oscillating in the middle of the trap between its original shape and an elliptical, yet highly focused, shape. When the charging becomes too high, confinement is lost, as shown in Figure 2m−p. The electron, though avoiding the tubes, manages to leak out by following the $x = 0$ and $y = 0$ lines.

Using the parameters of Figure 2i−l, we further investigate *focusing* of electronic wave packets. Figure 3 presents four frames of the wave function squared starting with an extended wave packet $\Psi(x, y, t = 0) = 1/(\pi^{1/2}\sigma)$, which is distributed *uniformly* within a circle of radius $\sigma = 95$ nm. We see that as time evolves the electron is drawn to, and gets localized at, the center of the trap. Only a small fraction of the probability density is seen to end up in the vicinity of the nanotubes.

The second panel of Figure 3 shows that focusing occurs for electrons that did not reside outside the trap region at $t = 0$. The total electron population within an extended circle of $r = 125$ nm goes down initially because the probability density outside the nanotube's region manages to leak out (···). However the density of electrons within $r = 35$ nm (−) and $r = 10$ nm (− −) goes up and remains stable on average, while undergoing some oscillations.

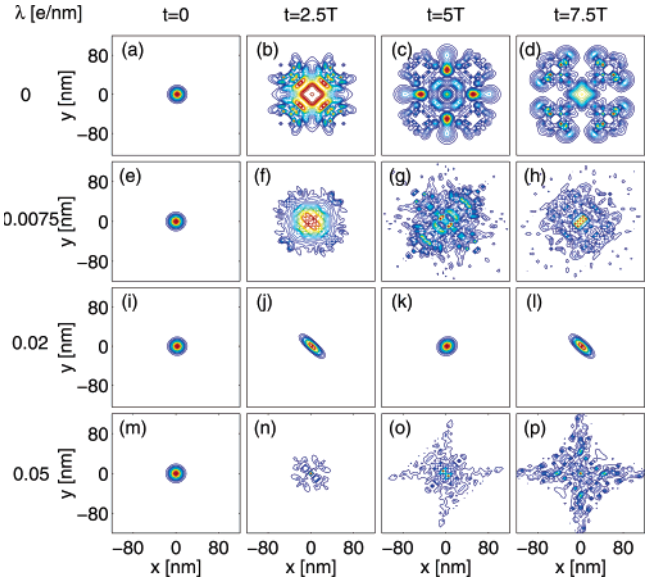

Figure 2. Electron's probability-density for different charging potentials. (a−d) $\lambda = 0$; (e−h) $\lambda = 0.0075$ e/nm; (i−l) $\lambda = 0.02$ e/nm; (m−p) $\lambda = 0.05$ e/nm. The calculation is performed in a $x-y$ 250 × 250 nm^2 lattice and for $\nu = 8.3\ 10^{11}$ Hz.

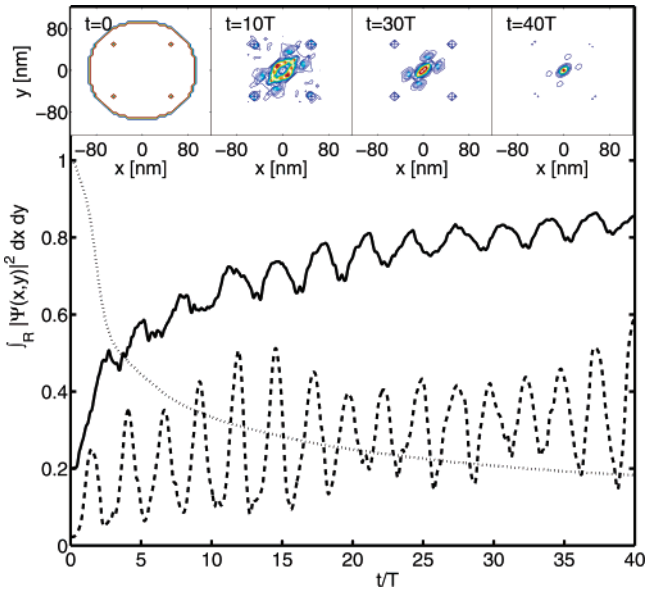

Figure 3. Focusing of an initially uniformly distributed highly extended wave function, for $\nu = 8.3\ 10^{11}$ Hz, $\lambda = 0.02$ e/nm. Top: probability-densities at different times. At $t = 0$ the wave packet is contained within a circle of $r = 95$ nm. Bottom: normalized population within smaller circles, $r < 35$ nm (−), $r < 10$ nm (− −). Total population contained in an $r < 125$ nm circle (···).

Figure 4 demonstrates trapping of an incoming electron with an initial nonzero mean momentum, $\Psi(x, y, t = 0) = \exp[-(x^2 + y^2)/2\sigma^2]e^{ik_x x + ik_y y}/\sqrt{\pi\sigma^2}$. The inset depicts the initial state, where the four small circles represent the tubes (not in scale). The main plot displays the trapped population ($r < 50$) for different initial momenta. We find that for $k_x = k_y = 0$ the electron does not reach the trap center, and it is fully absorbed at the right end (−). Effectively, this is because the electron cannot overcome the barrier encircling the trap, see Figure 6. For higher velocities, corresponding

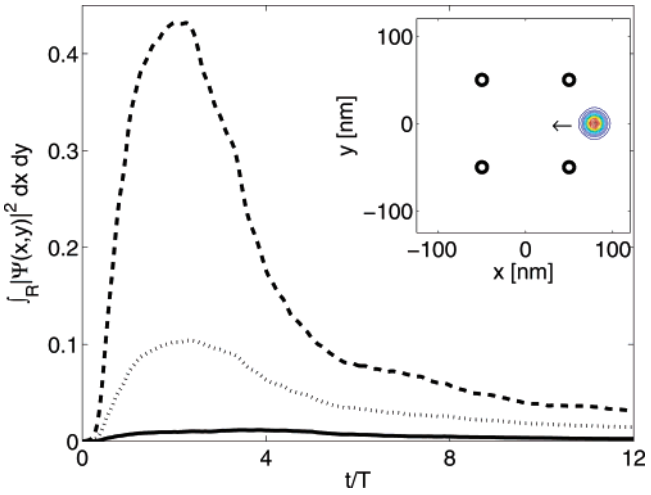

Figure 4. Trapping of a wave packet with an initial mean momentum. Main plot: population at the trap center ($r < 50$ nm) at different times, $k_x = 0$ (−); $k_x = -10^{-2}$ Å^{-1} (···); $k_x = -2\ 10^{-2}$ Å^{-1} (− −). $k_y = 0$, $\lambda = 0.02$ e/nm, and $\nu = 8.3\ 10^{11}$ Hz in all cases. Inset: the initial wave packet ($\sigma = 10.5$ nm) and the four tubes.

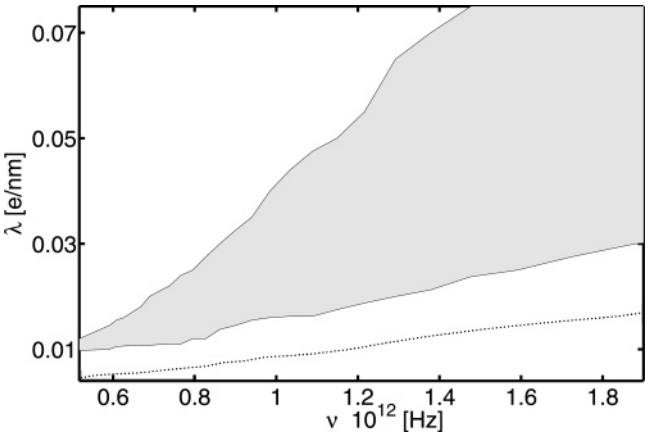

Figure 5. Stability map of the nano-trap. Trapping exists in the shaded area. The dotted line marks the lower border of the stability region when the contribution of the image potential is removed from the Hamiltonian. This removal has no effect on the upper border line.

to kinetic energies in the millielectronvolt range, part of the wave packet gets absorbed at the right side, but a significant portion reaches the trap center (···, − −). An important mechanism for relaxing the electron's momentum is via the excitation of the tube's vibrational modes.[4,16] This mechanism is not considered here, and high-energy electrons simply pass across the system. This explains the initial rise at $t/T \approx 2$, followed by a large loss of population at the left end.

A full characterization of the trap is presented in Figure 5 where the stability diagram for different frequencies and charging potentials is provided. The diagram was generated by propagating for long times ($\sim 10T$) initially localized or unlocalized wave packets and recording whether at the end of the integration time the wave function remains confined at the trap center. We ascertained that the results are independent of the wave packet's initial shape. Note that because of the image potential the range of stability is

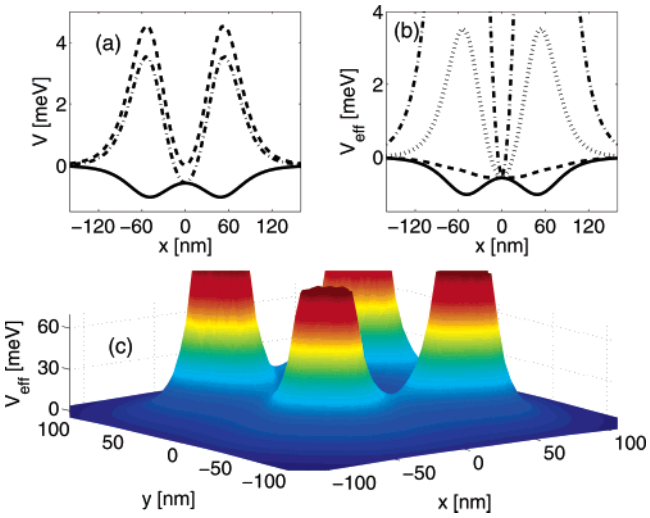

Figure 6. Effective trapping potentials for $\nu = 8.3\ 10^{11}$ Hz. (a) V_0 (−); V_{av} (− −); $V_{eff} = V_0 + V_{av}$ (− · −); $y = 0$, $\lambda = 0.02$ e/nm. (b) V_{eff} for $y = 0$, $\lambda = 0$ (−), 0.0075 e/nm (− −), 0.02 e/nm (···), 0.05 e/nm (− · −). The potential goes up to 30 meV. (c) Two-dimensional plots of $V_{eff}(x, y)$ for $\lambda = 0.05$ e/nm. The potential, which on the tube's surface is as high as 10 eV, is truncated at 60 meV.

decreased. This effect ultimately limits the operation of very small traps to $d > 10$ nm. Using eqs 7−8 we can easily generate such diagrams for different spatial dimensions. The trap stability can be also studied as a function of an additional dc voltage, as is usually done in conventional Paul traps.[6]

The behavior demonstrated here can be viewed as the quantum mechanical analogue of the classical concept of "dynamic stabilization".[22] It can be described using time-independent "effective potentials",[23] resulting from the expansion of $V_T(x, y, t)$ as a power series in Ω^{-2} and retaining the lowest order term, to obtain

$$V_{eff}(x, y) = V_0(x, y) + V_{av}(x, y),$$

$$V_{av}(x, y) = \frac{1}{4m_e\Omega^2} \sum_{q=x,y} \left(\frac{\partial V_Q(x, y)}{\partial q} \right)^2 \quad (9)$$

In Figure 6a, we depict the V_0, V_{av}, and V_{eff} potentials along $y = 0$. Although V_0 is minimal in the proximity of the nanotubes, V_{av} has a single minimum at the center of the trap, separated from the tubes by potential barriers. Far away from the rods, both potentials go to zero. Whether the minima of the *effective* potential is located at the trap center or around the tubes depends on the strength of the charging potential as shown in panel b.

Using the notion of the effective potential, one can readily understand the evolution of the wave packets depicted in Figure 2. In the absence of ac charging, only the image potential contributes, and the electron leaks to the tubes (a−d). For small charging values, the effective potential is wide and shallow, leading to a weak stabilization of the electron at the center (e−h). A further increase of the charge density yields a relatively deep effective potential where the electron can localize for long times. Tunneling outside is prohibited

because of the high barriers encircling the well (i−l). For very high ac charging, the electron leakage shown in (m−p) can now be understood as a tunneling process through the barriers. As demonstrated in Figure 6b, it is caused by the narrowness of the effective potential that pushes the eigenstates close to the barrier maximum. Thus, the resonance lifetimes of the effective-potential states can also be used for estimating the trap's regions of stability.

Finally, we note that an *axial* localization of the electron in the trap results naturally from the potential barriers imposed by the tube's end caps.[17] This causes the electron to oscillate in both radial and axial directions at drastically different frequencies. Although the radial vibrational frequency is ∼500 GHz, $\nu_z \approx 10$ GHz for the axial motion.[17] Strong axial confinement can be also achieved by applying a dc repulsive field on additional ring-shaped electrodes at the tube's ends.[6]

A single trapped electron is a promising candidate for a variety of quantum-information applications utilizing its spin states, the *anharmonic* quasienergy spectrum,[24] and its coupling to the nanowires mechanical modes.[4] Its dynamics can be manipulated either by magnetic fields or through coherent laser excitations. Of even greater interest would be *arrays* of electrons[25] trapped by a 2D lattice[15] of quartets of nano-traps of the type described here. Such arrays can be used as a set of entangled q-bits, where the degree of entanglement would be controlled by varying the ac charging, thereby allowing a greater or lesser portion of the electronic population to leak into neighboring cells and interact with other electrons confined there.

Acknowledgment. This project was supported by the Feinberg graduate school of the Weizmann Institute.

References

(1) Ghosh, P. K. *Ion Traps*; Clarendon Press: Oxford, 1995.
(2) Dehmelt, H. *Rev. Mod. Phys.* **1990**, *62*, 525.
(3) Cirac, J. I.; Zoller, P. *Phys. Rev. Lett.* **1995**, *74*, 4091.
(4) (a) Tian, L.; Zoller, P. *Phys. Rev. Lett.* **2004**, *93*, 266403-1. (b) Hensinger, W. K.; Utami, D. W.; Goan, H.-S.; Schwab, K.; Monroe, C.; Milburn, G. J. *Phys. Rev. A* **2005**, *72*, 041405(R).
(5) Brown, L. S.; Gabrielse, G. *Rev. Mod. Phys.* **1986**, *58*, 233.
(6) Paul, W. *Rev. Mod. Phys.* **1990**, *62*, 531.
(7) (a) Tu, Y.; Lin, Y.; Ren, Z. F. *Nano Lett.* **2003**, *3*, 107. (b) Yu, Z.; Li, S.; Burke, P. J. *Chem. Mater.* **2004**, *16*, 3414.
(8) Maeda, Y.; Kimura, S.-i.; Kanda, M.; Hirashima, Y.; Hasegawa, T.; Wakahara, T.; Lian, Y.; Nakahodo, T.; Tsuchiya, T.; Akasaka, T.; Lu, J.; Zhang, X.; Gao, Z.; Yu, Y.; Nagase, S.; Kazaoui, S.; Minami, N.; Shimizu, T.; Tokumoto, H.; Saito, R. *J. Am. Chem. Soc.* **2005**, *127*, 10287.
(9) An, L.; Fu, Q.; Lu, C.; Liu, J. *J. Am. Chem. Soc.* **2004**, *126*, 10520.
(10) (a) Zhang, X. Y.; Zhang, L. D.; Chen, W.; Meng, G. W.; Zheng, M. J.; Zhao, L. X.; Phillipp, F. *Chem. Mater.* **2001**, *13*, 2511. (b) Oshima, Y.; Onga, A.; Takayanagi, K. *Phys. Rev. Lett.* **2003**, *91*, 205503.
(11) Cheng, C.; Gonela, R. K.; Gu, Q.; Haynie, D. T. *Nano Lett.* **2005**, *5*, 175.
(12) (a) Burke, P. J. *Solid-State Electron.* **2004**, *48*, 1981. (b) Yu, Z.; Burke, P. J. *Nano Lett.* **2005**, *5*, 1403.
(13) Meng, G.; Jung, Y. J.; Cao, A.; Vajtai, R.; Ajayan, P. M. *Proc. Natl. Acad. Sci.* **2005**, *102*, 7074.
(14) Granger, B. E.; Král, P.; Sadeghpour, H. R.; Shapiro, M. *Phys. Rev. Lett.* **2002**, *89*, 135506-1.
(15) Segal, D.; Granger, B. E.; Sadeghpour, H. R.; Král, P.; Shapiro, M. *Phys. Rev. Lett.* **2005**, *94*, 016402.
(16) Segal, D.; Král, P.; Shapiro, M. *Surf. Sci.* **2005**, *577*, 86.
(17) Segal, D.; Král, P.; Shapiro, M. *Phys. Rev. B* **2004**, *69*, 153405.
(18) Slater, J. C.; Frank, N. H. *Electromagnetism*; McGraw-Hill: New York, 1947.
(19) Brown, L. S. *Phys. Rev. Lett.* **1991**, *66*, 527.
(20) Balakrishnan, N.; Kalyanaraman, C.; Sathyamurthy, N. *Phys. Rep.* **1997**, *280*, 79.
(21) Neuhasuer, D.; Baer, M. *J. Chem. Phys.* **1989**, *90*, 4351.
(22) Landau, D. L.; Lifshitz, E. M. *Mechanics*; Pergamon Press: Oxford, 1976.
(23) (a) Gilary, I.; Moiseyev, N.; Rahav, S.; Fishman, S. *J. Phys. A: Math. Gen.* **2003**, *36*, L409. (b) Rahav, S.; Gilary, I.; Fishman, S. *Phys. Rev. A* **2003**, *68*, 013820.
(24) Mancini, S.; Martins, A. M.; Tombesi, P. *Phys. Rev. A* **2000**, *61*, 012303.
(25) Ciaramicoli, G.; Marzoli, I.; Tombesi, P. *Phys. Rev. Lett.* **2003**, *91*, 017901.

NL060560H